

THE HALO MASS-BIAS REDSHIFT EVOLUTION IN THE Λ CDM COSMOLOGYS. BASILAKOS¹, M. PLIONIS^{2,3}, C. RAGONE-FIGUEROA^{4,5}*Draft version September 14, 2021*

ABSTRACT

We derive an analytic model for the redshift evolution of linear-bias, allowing for interactions and merging of the mass-tracers, by solving a second order differential equation based on linear perturbation theory and the Friedmann-Lemaître solutions of the cosmological field equations. We then study the halo-mass dependence of the bias evolution, using the dark matter halo distribution in a Λ CDM simulation in order to calibrate the free parameters of the model. Finally, we compare our theoretical predictions with available observational data and find a good agreement. In particular, we find that the bias of optical QSO's evolve differently than those selected in X-rays and that their corresponding typical dark matter halo mass is $\sim 10^{13} h^{-1} M_{\odot}$ and $\gtrsim 5 \times 10^{13} h^{-1} M_{\odot}$, respectively.

Subject headings: cosmology: theory – dark matter – galaxies: halos – galaxies: formation – large-scale structure of universe – methods: N-body simulations.

1. INTRODUCTION

The distribution of matter on large scales, based on different extragalactic objects, can provide important constraints on models of cosmic structure formation. However, a serious problem that hampers such a straight forward approach is our limited knowledge of how luminous matter traces the underlying mass distribution. It is well known that the large scale clustering pattern of different extragalactic objects (galaxies, AGN, clusters, etc) trace the underlying dark matter distribution in a biased manner (Kaiser 1984; Bardeen et al. 1986). Such a biasing is assumed to be statistical in nature; with galaxies and clusters being identified as high peaks of an underlying, initially Gaussian, random density field. Furthermore, the biasing of galaxies with respect to the dark matter distribution was also found to be a necessary ingredient of Cold Dark Matter (CDM) models of galaxy formation in order to reproduce the observed galaxy distribution (eg. Davis et al. 1985; Cole & Kaiser 1989; Benson et al. 2000).

Furthermore, the bias redshift evolution is very important in order to relate observations with models of structure formation and it has been shown that the bias factor, $b(z)$, is a monotonically increasing function of redshift. Indeed, Mo & White (1996) and Matarrese et al. (1997) have developed a model for the evolution of the correlation bias, defined as the ratio of the halo to the mass correlation function, the so called galaxy merging bias model. This model takes into account, via the Press-Schechter formalism, the collapse of different mass halos at the different epochs. In this framework and at high z 's one finds, in the EdS universe, that $b(z) - 1 \propto (1+z)$ (see also Sheth et al. 2001). According to Matarrese et al. (1997), if the only halos that exist at any epoch are those that have just formed via a merging process of smaller halos then the bias evolution, in the high density peak limit, becomes $b(z) \propto (1+z)^2$ (see also Bagla 1998). There are many studies of the merging bias model in the context of a Λ

cosmology (e.g. Jing 1998; Sheth & Tormen 1999; Sheth, Mo & Tormen 2001), while the bias has been found to be a key ingredient of the halo model (e.g. Peacock & Smith 2000; Seljak 2000; Ma & Fry 2000).

The so-called galaxy conserving bias model (Nusser & Davis 1994; Fry 1996; Tegmark & Peebles 1998; Hui & Parfrey 2007) assumes only that the different mass-tracer (acting as “test particles”) fluctuation field is proportional to that of the underlying mass and it predicts a bias evolution according to: $b(z) = 1 + (b_0 - 1)(1+z)$ for $\Omega_m = 1$, where b_0 is the bias factor at the present time. Coles, Melott & Munshi (1999) have developed a bias model within the hierarchical clustering scenario which gives interesting scaling relations for the galaxy bias. Another approach was proposed by Basilakos & Plionis (2001; 2003), in which the linear bias evolution was described via the solution of a second order differential equation, derived using linear perturbation theory and the basic cosmological equations. Also, in this model the mass tracer population is assumed to be conserved in time.

In this paper we extend the original Basilakos & Plionis linear and scale-independent bias evolution model to include the effects of an evolving mass-tracer population, possibly due to interactions and merging. We then derive the dependence of the linear-bias evolution on halo mass, with the help of N-body simulations, in the framework of the concordance Λ CDM cosmological model. Additionally we compare our model with observations.

2. LINEAR BIAS EVOLUTION MODEL

In this section we describe our general linear bias evolution model which is based on linear perturbation theory in the matter dominated epoch (eg. Peebles 1993), either assuming that the mass-tracer population is conserved in time or that it evolves according to a $(1+z)^\nu$ law.

2.1. Case 1: Conservation of Mass-tracer Population

¹ Research Center for Astronomy & Applied Mathematics, Academy of Athens, Soranou Efessiou 4, GR-11527 Athens, Greece

² Institute of Astronomy & Astrophysics, National Observatory of Athens, Palaia Penteli 152 36, Athens, Greece

² Instituto Nacional de Astrofísica Óptica y Electrónica, AP 51 y 216, 72000, Puebla, Pue, México

⁴ Grupo IATE-Observatorio Astronómico, Laprida 854, Córdoba, Argentina

⁵ Consejo de Investigaciones Científicas y Técnicas de la Rep'ública Argentina, Córdoba, Argentina

In Basilakos & Plionis (2001; 2003) we have assumed that in the evolution of the linear bias the effects of non-linear gravity and hydrodynamics (merging, feedback mechanisms etc) can be ignored (eg. Fry 1996; Tegmark & Peebles 1998; Catelan et al. 1998). Then, using the linear perturbation theory we obtained a second order differential equation which describes the evolution of the linear bias factor, b , between the background matter and the mass-tracer fluctuation field:

$$\ddot{y}\delta + 2(\dot{\delta} + H\delta)\dot{y} + 4\pi G\rho_m\delta y = 0, \quad (1)$$

where $b = y + 1$ and $\delta(t) \propto D(t)$. Note that $D(t)$ is the linear growing mode (scaled to unity at the present time), useful expressions of which can be found for the Λ cosmology in Peebles et al. (1993):

$$D(z) = \frac{5\Omega_m E(z)}{2} \int_z^\infty \frac{(1+x)}{E^3(x)} dx, \quad (2)$$

and for the quintessence models in Silveira & Waga (1994), Wang & Steinhardt (1998) and Basilakos (2003). The solution of eq.(1) provided our bias evolution model (Basilakos & Plionis 2001). The solution for the different cosmological model enter through the different behavior of $D(t)$ and $H(t)$.

In order to transform equation (1) from time to redshift, we utilized the following expressions:

$$\frac{dt}{dz} = -\frac{1}{H_0 E(z)(1+z)} \quad (3)$$

$$E(z) = [\Omega_m(1+z)^3 + \Omega_\Lambda]^{1/2}, \quad (4)$$

with Ω_m being the density parameter at the present time, which satisfies $\Omega_\Lambda = 1 - \Omega_m$. Taking into account the latter transformations, the basic differential equation for the evolution of the linear bias parameter takes the following form:

$$\frac{d^2 y}{dz^2} - P(z)\frac{dy}{dz} + Q(z)y = 0 \quad (5)$$

with relevant factors,

$$P(z) = \frac{1}{1+z} - \frac{1}{E(z)} \frac{dE(z)}{dz} - \frac{2}{D(z)} \frac{dD(z)}{dz} \quad (6)$$

and

$$Q(z) = \frac{3\Omega_m(1+z)}{2E^2(z)}. \quad (7)$$

The general solution as a function of redshift for flat cosmological models ($\Omega_m + \Omega_\Lambda = 1$) was found to be (Basilakos & Plionis 2001):

$$b(z) = C_1 E(z) + C_2 E(z)I(z) + 1, \quad (8)$$

with

$$I(z) = \int_z^\infty \frac{(1+x)^3}{E^3(x)} dx. \quad (9)$$

The integral of equation (9) is elliptic and therefore its solution, in the redshift range $[z, +\infty)$, can be expressed as a hyper-geometric function:

$$I(z) \propto (1+z)^{-1/2} F\left[\frac{1}{6}, \frac{3}{2}, \frac{7}{6}, -\frac{\Omega_\Lambda}{\Omega_m(1+z)^3}\right]. \quad (10)$$

Note that the first term in the right-hand side of eq.(8), which is the dominant one, has an approximate redshift dependence $\sim (1+z)^{3/2}$ while the second term has a dependence $\sim (1+z)$.

In Basilakos & Plionis (2001) we compared this bias evolution model with the halo merging model (eg. Mo & White 1996; Matarrese et al. 1997) for $z \leq 3$ and found a very good consistency, once we fitted the integration constants C_1, C_2 by evaluating our model to two different epochs. Also in Basilakos & Plionis (2003) we compared our Λ CDM solution, evaluated at $z = 0$ and $z = 3$ using the Hubble Deep Field (HDF) results (Arnouts et al. 2002), with the Matarrese et al (1997) model and again found a good consistency.

However, the consistent comparison of our bias evolution model with the available observational and numerical data is only after we normalize our model to two different epochs, given by the data. In other words there is no independent normalization of our bias evolution curves.

2.2. Case 2: Evolving Mass-tracer Population

The assumption used in the previous section, that the mass-tracer number density is conserved in time, should be a gross oversimplification, since in most galaxy formation models it is expected that interactions and merging is very important at early epochs.

We now drop this assumption by allowing a contribution from the corresponding interactions among the mass tracers and thus an evolution of the mass-tracer population. We derive again the corresponding equation (1), starting from the continuity equation and introducing an additional time-dependent term, $\Psi(t)$, which we associate with the effects of interactions and merging of the mass tracers. We also make the same assumption, as in our original formulation, that the tracers and the underlying mass distribution share the same velocity field. Then:

$$\dot{\delta} + \nabla u \simeq 0 \quad \text{and} \quad \dot{\delta}_g + \nabla u + \Psi(t) \simeq 0, \quad (11)$$

from which we obtain

$$\dot{\delta} - \dot{\delta}_g = \Psi. \quad (12)$$

Although we do not have a fundamental theory to model the time-dependent $\Psi(t)$ function, according to the notations of Simon (2005), it appears to depend on the tracer number density and its logarithmic derivative as well as on the tracer overdensity: $\Psi(t) \propto \Psi(\bar{n}, (1 + \delta_g)d \ln \bar{n}/dt)$ (see eq. 10 of Simon 2005 and our appendix).

Now, since we are dealing with linear biasing, we have $\delta_g = b\delta$ and using $b = y + 1$, we get that $d(y\delta)/dt = -\Psi$. Differentiating twice we then have: $\ddot{y}\delta + 2\dot{y}\dot{\delta} + y\ddot{\delta} = -\dot{\Psi}$. Solving for $y\ddot{\delta}$, using the fact that $y\dot{\delta} = -\dot{y}\delta - \Psi$ and utilizing the differential time-evolution equation of δ (eg. Peebles 1993):

$$\ddot{\delta} + 2H\dot{\delta} - 4\pi G\rho_m\delta = 0 \quad (13)$$

we finally obtain:

$$\ddot{y}\delta + 2(\dot{\delta} + H\delta)\dot{y} + 4\pi G\rho_m\delta y = -2H\Psi - \dot{\Psi} \quad (14)$$

which is the corresponding equation (1) for the case of interactions among the tracers.

If we transform the latter equation from time to redshift the basic differential equation becomes:

$$\frac{d^2 y}{dz^2} - P(z)\frac{dy}{dz} + Q(z)y = f(z) \quad (15)$$

with

$$f(z) = \frac{(1+z)\Psi'(z)E(z) - 2E(z)\Psi(z)}{H_0 D(z)} \quad (16)$$

where the prime denotes derivative with respect to redshift.

Therefore, if one is able to find a partial solution y_p of eq. (15), then due to the fact that we know already the solutions [$E(z)$ and $E(z)I(z)$ in section 2.1] for the homogeneous case, the general solution for the interactive case should satisfy the following formula:

$$y(z) = \mathcal{C}_1 E(z) + \mathcal{C}_2 E(z)I(z) + y_p(z) . \quad (17)$$

Using some basic elements of the differential equation theory, the corresponding partial solution becomes

$$y_p(z) = E(z) \int_0^z \frac{f(x)E^2(x)I(x)}{(1+x)^3} dx - E(z)I(z) \int_0^z \frac{f(x)E^2(x)}{(1+x)^3} dx . \quad (18)$$

It is obvious that if the interaction among the tracers is negligible ($\Psi \simeq 0$) then $y_p \simeq 0$, as it should.

In order to proceed we need to define the functional form of the interaction term $\Psi(z)$ which is not an easy task to do. Due to the absence of a physically well-motivated fundamental theory, we parametrize the interaction term utilizing a standard evolutionary form:

$$\Psi(z) = AH_0(1+z)^\nu \quad (19)$$

implying that

$$f(z) = A(\nu - 2) \frac{(1+z)^\nu E(z)}{D(z)} , \quad (20)$$

where A and ν are positive parameters (to be determined from simulations see next section). This is a reasonable approach since it can be shown that indeed our $\Psi(z)$ term has such a dependence (see appendix). From a mathematical point of view, we have that for $\nu > 2$ the bias evolution becomes stronger than in the case of no interactions, especially at high redshifts, which means that due to the merging processes the halos (of some particular mass) correspond to higher peaks of the underlying density field with respect to equal mass halos in the non-interacting case. On the other hand, the $\nu < 2$ case corresponds to the destruction of halos of a particular mass, which results into a lower-rate of bias evolution with respect to the non-interacting case. Now, for the limiting case with $\nu = 2$ we obtain $y_p = 0$, implying no contribution of the interacting term to the bias evolution solution, as in the case with $\Psi(t) = 0$, which can be interpreted as the case where the destruction and creation processes are counter-balanced.

3. PARAMETRIZING THE BIAS EVOLUTION MODEL USING N-BODY SIMULATIONS

Our analytical approach gives a family of bias curves with four unknown parameters ($\mathcal{C}_1, \mathcal{C}_2, A, \nu$). In order to obtain the behavior of $b(z)$ we need to somehow evaluate these constants for different halo-masses (since different halo-masses result in different $b(0)$ and different rate of bias evolution) and we do so by using a Λ CDM, dark matter only, simulation.

3.1. Simulation Data

The simulation volume is of a $500 h^{-1}$ Mpc cube in which a random realization of the concordance Λ CDM ($\Omega_m = 0.3$, $\Omega_\Lambda = 0.7$, $h = 0.72$ and $\sigma_8 = 0.9$) power spectrum was generated with 512^3 particles (Ragone-Figueroa

& Plionis 2007). The simulation was performed with an updated version of the parallel Tree-SPH code GADGET2 (Springel 2005). The particle mass is $m_p \geq 7.7 \times 10^{10} h^{-1} M_\odot$ comparable to the mass of one single galaxy. The halos are defined using a FoF algorithm with a linking length $l = 0.17 \langle n \rangle^{-1/3}$, where $\langle n \rangle$ is the mean particle density. This linking length corresponds to an overdensity $\simeq 330$ at the present epoch ($z = 0$).

We estimate the bias redshift evolution of the different dark mass halos, with respect to the underlying matter distribution, by measuring their relative fluctuations in spheres of radius $8 h^{-1}$ Mpc, according to:

$$b(M, z) = \frac{\sigma_{8,h}(M, z)}{\sigma_{8,m}(z)} , \quad (21)$$

where the subscripts h and m denote halos and the underlying mass, respectively. The values of $\sigma_{8,h}(M, z)$, for halos of mass M , are computed at different redshifts, z , by:

$$\sigma_{8,h}^2(M, z) = \left\langle \left(\frac{N - \bar{N}}{\bar{N}} \right)^2 \right\rangle - \frac{1}{\bar{N}} , \quad (22)$$

where \bar{N} is the mean number of such halos in spheres of $8 h^{-1}$ Mpc radius and the factor $1/\bar{N}$ is the expected Poissonian contribution to the value of $\sigma_{8,h}^2$. Similarly, we estimate at each redshift the value of the underlying mass $\sigma_{8,m}$. In order to measure $\sigma_{8,j}^2$ we randomly place N_{rand} sphere centers in the simulation volume, such that the sum of their volumes is equal to 1/8 of the simulation volume ($N_{\text{rand}} \simeq 7500$). This is to ensure that we are not oversampling the available volume, in which case we would have been multiply sampling the same halo or mass fluctuations. The uncertainties reflect the dispersion in the distribution of $\sigma_{8,j}^2$, taking 20 bootstrap resamplings of the halo sample. Note, that these errors do not take into account the uncertainties introduced by cosmic variance, although for the majority of the halo mass ranges investigated it should be negligible, due to the size of the simulation volume. Nevertheless, we verified this by investigating the effects of cosmic variance on the value of σ_8 for volumes 8 times smaller than our simulation box and found them to be significantly smaller than the corresponding bootstrap errors.

For our present analysis we use 10 different redshift snapshots, spanning the range: $0 \leq z \leq 5$ and five different halo mass intervals:

- Sample S_1 : $7.7 \times 10^{11} h^{-1} M_\odot \leq M \leq 10^{13} h^{-1} M_\odot$
- Sample S_2 : $1 \times 10^{13} h^{-1} M_\odot < M \leq 3 \times 10^{13} h^{-1} M_\odot$
- Sample S_3 : $3 \times 10^{13} h^{-1} M_\odot < M \leq 6 \times 10^{13} h^{-1} M_\odot$
- Sample S_4 : $6 \times 10^{13} h^{-1} M_\odot < M \leq 1 \times 10^{14} h^{-1} M_\odot$
- Sample S_5 : $1 \times 10^{14} h^{-1} M_\odot < M \leq 4 \times 10^{14} h^{-1} M_\odot$

In Figure 1 we present with dots the simulation $b(M, z)$ results for the different subsamples (solid points S_1 , open points S_2 , crosses S_3 , solid squares S_4 and open squares S_5). As it is expected, the biasing is a monotonically increasing function of redshift with its evolution being significantly stronger for larger halo masses (eg. Kauffmann et al. 1999; Somerville et al 2001 and references therein). By solid curves we present our bias evolution models (case's

1 and 2 at the left and right panels, respectively), which have been fitted to the N-body results (see below).

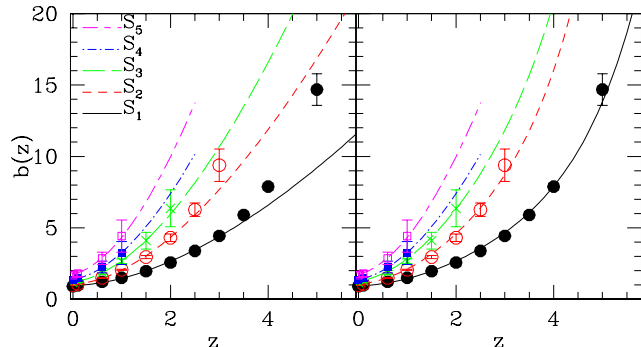


FIG. 1.— The bias z -evolution for different halo masses in a concordance Λ CDM simulation (points). Continuous lines represent our bias evolution model, fitted to the simulation results: (*Case 1* is shown in the left panel and *Case 2* in the right panel). Note that the different continuous lines corresponds to different halo masses and thus to different values of the fitted model parameters, shown in Table 1.

3.2. Fitting our Model $b(z)$

Firstly we fit to the simulation data our (*Case 1*) model, where the mass tracers population is conserved in time. To do so we utilize a standard χ^2 likelihood procedure and compare the measured bias evolution, $b(M, z)$, with that expected from our theoretical approach (see eq. 8). We define the likelihood estimator⁶ as: $\mathcal{L}(\mathbf{c}) \propto \exp[-\chi^2(\mathbf{c})/2]$ with:

$$\chi^2(\mathbf{c}) = \sum_{i=1}^n \left[\frac{b^i(M, z) - b^i(\mathbf{c}, z)}{\sigma^i} \right]^2, \quad (23)$$

where \mathbf{c} is a vector containing the parameters that we want to fit and σ_i is the derived uncertainty (see previous section). Note, that in this case $\mathbf{c} = (\mathcal{C}_1, \mathcal{C}_2)$. We sample the various parameters as follows: $\mathcal{C}_1 \in [0, 25]$ and $\mathcal{C}_2 \in [-2, 4]$ in steps of 0.01.

In Fig. 1 (left panel), we plot our derived bias evolution fits (lines) to the simulation data (points) to find that indeed they compare very well for $z \lesssim 2.5 - 3$. However, it appears that at larger redshifts the simulation halo bias evolves more rapidly than what our (*Case 1*) model predicts, especially for the low mass halos (see S_1, S_2 and S_3 subsamples), which of course should be attributed to the assumption of halo number density conservation. However, it is evident that this model describes well the bias evolution for the high mass halos (see samples S_4 and S_5), since such high-mass halos form quite late in the evolution of structure formation processes.

These results strongly indicate that the interactions among the relative low mass tracers at large redshifts play an important role in the evolution of halo biasing. We now perform our likelihood analysis for the *Case 2* model, i.e., using the corresponding vector: $\mathbf{c} = (\mathcal{C}_1, \mathcal{C}_2, A, \nu)$. We sample the (A, ν) parameters as follows: $A \in [10^{-3}, 10^{-2}]$ in steps of 10^{-3} ; and $\nu \in [2, 3]$ in steps of 0.02. The procedure is applied only for the lower mass halos (see S_1, S_2 and S_3 subsamples). The resulting best fit parameters and

⁶ Likelihoods are normalized to their maximum values.

⁷ For $z = 0$ we get $b_0 = b(0) = 1 + \mathcal{C}_1 + \mathcal{C}_2 I(0)$. Note that for the concordance model $\Omega_m = 1 - \Omega_\Lambda = 0.3$ we have $I(0) \simeq 9.567$

the zero-point bias, b_0 ⁷, for the five subsamples, are presented in Table 1, while we plot the results, as continuous lines, in the right panel of figure 1.

Our *Case 2* model fits extremely well the numerical simulation results even at high redshifts, which implies that our modification of the test-particle bias solution, to take into account interactions among mass-tracers, is an extremely good approximation to the more elaborate halo bias evolution solutions, based on the Press-Schechter formalism. Note also that the derived values of the constants of integration, $(\mathcal{C}_1, \mathcal{C}_2)$, are very similar in both of our models (*Case 1* and *Case 2*).

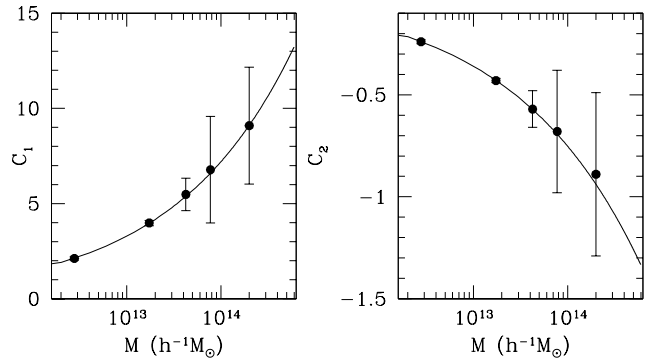


FIG. 2.— The relation between the measured constants and the median of each halo mass interval (\mathcal{C}_1 and \mathcal{C}_2 in the *right* and *left* panels, respectively). The corresponding fits, in both panels, are given by eq.(24).

We would like to caution the reader that the fitted parameters, tabulated in Table 1, are based on a concordance Λ CDM simulation with a high σ_8 ($= 0.9$) normalization. We have investigated the sensitivity of these parameters to the power-spectrum normalization by running a *WMAP3* normalized ($\sigma_8 = 0.75$) simulation (but of a smaller box size: $L = 250 h^{-1}$ Mpc) and found small differences and only for the \mathcal{C}_1 and $b(0)$ parameters. We find for the *WMAP3* normalization case that the value of \mathcal{C}_1 and $b(0)$ are higher by $\sim 4\%$ and $\sim 6\%$, respectively, with respect to those presented in Table 1. On the other hand, the choice of the value of Ω_m affects only the constant \mathcal{C}_2 , which for the case of different flat cosmologies should be multiplied by a factor $(\Omega_m/0.3)^{3/2}$ (see Basilakos & Plionis 2001).

Now, in order to derive a generic halo-mass dependent formula of our bias evolution model, within the Λ CDM model, we correlate the constants $\mathcal{C}_1, \mathcal{C}_2$, with the median mass of the corresponding halo sub-samples and find the following fits (shown in figure 2):

$$\mathcal{C}_{1,2}(M) \simeq \alpha_{1,2} \left(\frac{M}{10^{13} h^{-1} M_\odot} \right)^{\beta_{1,2}}, \quad (24)$$

where $\alpha_1 = 3.29 \pm 0.21$, $\beta_1 = 0.34 \pm 0.07$ and $\alpha_2 = -0.36 \pm 0.01$, $\beta_2 = 0.32 \pm 0.06$ are the corresponding best values with their 1σ uncertainties.

Finally, we need to emphasize that with our current model, assuming also that the extragalactic mass tracers (clusters, galaxies, X-ray sources, etc.) are hosted by a halo of a given mass, it is straightforward to derive ana-

lytically their bias evolution behavior.

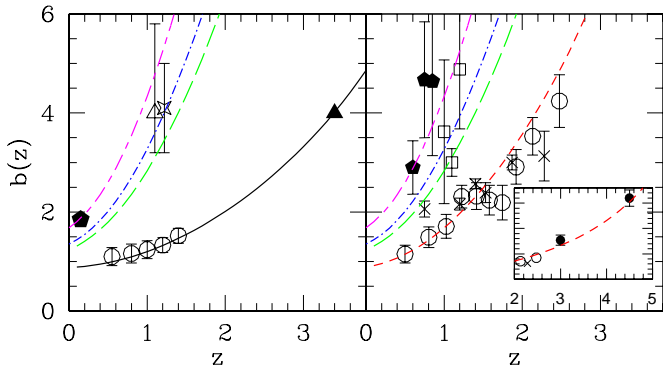


FIG. 3.— Comparison of our $b(z)$ model with different observational data. Different line types represent different halo masses (see section 3.1). *Left Panel:* optical galaxies (open points), Lyman break galaxies (solid triangle), EROs (star), DRGs (open triangle) and 2dF radio sources (filled pentagon). *Right Panel:* optically selected quasars (open points and crosses), soft and hard X-ray point sources (open squares and solid diamonds). In the insert we plot, as solid points, the high- z SSRS DR5 QSOs and the same $b(z)$ model that fits their lower redshift counterparts (ie., $M \simeq 10^{13} h^{-1} M_{\odot}$).

4. COMPARISON WITH OBSERVATIONS & OTHER BIAS MODELS

We investigate the extent to which our bias-evolution model can fit recent observational data of different extragalactic sources and which is the DM halo mass for which such a comparison is successful. In performing such a comparison we implicitly assume that, on average, each class of extragalactic sources is related to DM haloes of some, specific, mass. Therefore, to the extent to which our model fits the data, we will be able to identify the (average) mass of the DM halo which the different extragalactic sources inhabit. We will also compare our model with other recent bias evolution models to show the extent to which they compare.

In the left panel of figure 3 we compare our theoretical prediction with observations using optical galaxies (open circles) from the VIMOS VLT Deep Survey (Marinoni et al. 2005). It is quite evident that our model (solid line), corresponding to a DM halo mass of $\sim 10^{12} h^{-1} M_{\odot}$, represents extremely well the z -dependence of the optical galaxy bias. It is quite interesting that the same $b(z)$ curve fits accurately the Lyman-break galaxies (solid triangle) at a redshift $z \geq 3$ (Steidel et al. 1998; Adelberger et al. 1998; Kashikawa et al. 2006).

Roche et al. (2002) using the ELAIS N2 field and Georgakakis et al. (2005) based on the PHOENIX deep survey find that the correlation length of the extremely red galaxies (EROs) lies in the interval $r_0 \simeq 10 - 17 h^{-1}$ Mpc for a slope $\gamma = 1.8$. Thus, the corresponding EROs bias value, derived using:

$$b(z) = \left(\frac{r_0}{r_{0,m}} \right)^{\gamma/2} D^{3+\epsilon}(z) \quad \text{with } \gamma = 1.8 \text{ \& } \epsilon = -1.2,$$

is $b \simeq 4.1 \pm 0.9$ at a redshift $z \simeq 1.2$ (shown as a star in the left panel of Fig. 3). While, Foucaud et al. (2007) find for the distant red galaxies (DRGs) in the UKIDSS Ultra Deep Survey, a bias parameter of $b = 4_{-0.8}^{+1.4}$ at a mean redshift of $z \simeq 1$ (see open triangle). Our model

bias-evolution curve that fits quite well both of these results (EROs and DRGs) is the one corresponding to a DM halo mass of $\sim 7.7 \times 10^{13} h^{-1} M_{\odot}$ (dot dashed line). For comparison we also show $b(z)$ curves for two more halo masses: $\sim 4.2 \times 10^{13} h^{-1} M_{\odot}$ (long dashed line) and $\sim 2 \times 10^{14} h^{-1} M_{\odot}$ (short long line).

Finally, Magliocchetti et al. (2004) find $b \simeq 1.85$ (see filled pentagon) for the 2dF radio galaxies at $z \leq 0.15$, corresponding to the model bias of a $\sim 10^{14} h^{-1} M_{\odot}$ DM halo.

In the right panel of figure 3 we compare the results of optical and X-ray selected AGNs with our $b(z)$ models. The bias evolution of optical quasars by Croom et al. (2005) and Myers et al. (2007) based on the 2dF QSOs (open circles) and the SDSS DR4 (crosses) survey, respectively, are well approximated by our $b(z)$ model for a DM halo of $\sim 10^{13} h^{-1} M_{\odot}$ (short dashed line). It is interesting to mention that also Croom et al. (2005), utilizing the Sheth, Mo & Tormen (2001) theoretical prescription, found that the median DM halo mass, for the expected quasar bias evolution, is $\sim 10^{13} h^{-1} M_{\odot}$ (Porciani, Magliocchetti, Norberg 2004; see also figure 7 of Negrello, Magliocchetti & de Zotti 2006; Hopkins et al. 2007).

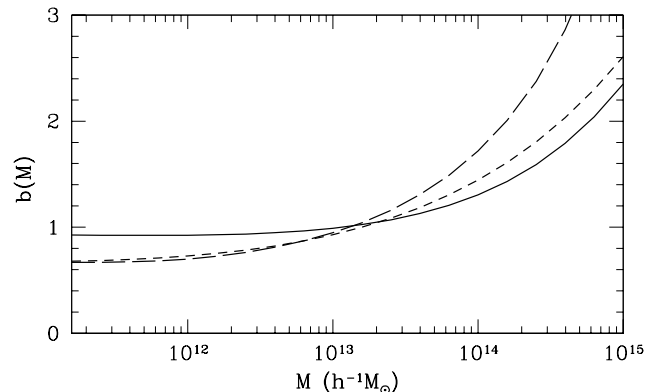


FIG. 4.— The bias parameter as a function of the halo mass at the present epoch. The solid line corresponds to our predictions, while the dashed and the long dashed lines to those of the Jing (1998) and Seljak & Warren (2004) models, respectively.

Recently, Shen et al. (2007) using the SDSS DR5 data found that the high redshift optical quasars ($2.9 \leq z \leq 5.4$) are more clustered than their $z \sim 1.5$ counterparts. The corresponding bias values (solid points in the insert plot) are fitted extremely well by the same model $b(z)$ function as their lower redshift counterparts (ie., for a DM halo mass of $\sim 10^{13} h^{-1} M_{\odot}$).

Finally, the relatively strong clustering results of X-ray selected AGNs, based on a variety of XMM and Chandra surveys (eg. Gilli et al. 2005; Basilakos et al. 2004; 2005; Puccetti et al. 2006; Miyaji et al. 2007), correspond to bias results shown in the right panel of figure 3 as open squares (soft band) and solid diamonds (hard band). The model $b(z)$ curves that fit these results correspond to halo masses $M > 5 \times 10^{13} h^{-1} M_{\odot}$, strongly suggesting that X-ray and optically selected AGNs do not inhabit the same DM halos.

From the previous comparisons it is evident that our bias evolution model (*Case 2*) describes well the bias behavior of different extragalactic sources.

We now turn to compare our generalized test-particle bias model (*Case 2*) with some recent merging bias models. As an example, in figure 4 we compare our solution to that of Jing (1998) and Seljak & Warren (2004) at $z = 0$. The corresponding functional $b(M)$ forms appear to be quite similar, although the predictions of Jing (1998) and Seljak & Warren (2004), with respect to our model, are lower by $\sim 20\%$ and higher by $\sim 15\%$ in the low and high-halo mass range, respectively. It is worth pointing out that for DM halo masses close to those related to optical galaxies, the Jing (1998) as well as the Seljak & Warren (2004) models predict a strongly anti-bias picture at the present epoch ($b_0 \sim 0.68$), which appears to be in disagreement with observational results which indicate that $b_0 \sim 1$ (eg. Verde et al. 2002; Lahav et al. 2002).

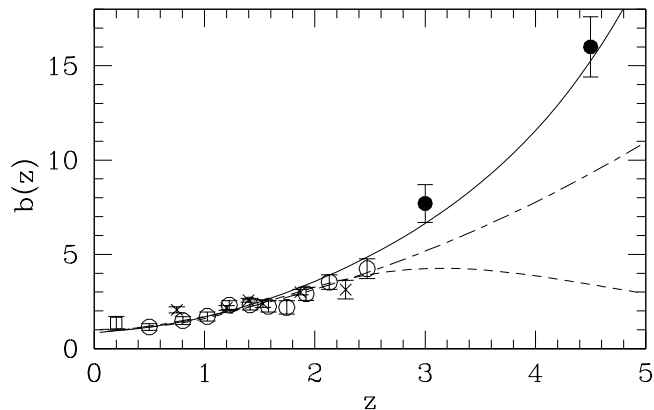


FIG. 5.— Comparison of our bias model for a DM halo mass of $10^{13} h^{-1} M_{\odot}$ (solid line) with the corresponding Croom et al (2005) empirical form (dot-dashed line) and the Hopking et al. (2007) model (dashed line). The points represent the optical QSO bias from the 2dF (open points), the SDSS DR4 (crosses) and the SDSS DR5 (solid points) surveys, while at $z \sim 0.2$ we plot the Asiago-ESO/RASS QSO survey results (Grazian et al. 2004).

Finally, in figure 5 we again plot the optical QSO bias, as a function of redshift (see also Fig. 3), together with some

bias-evolution model predictions. Our generalized solution for a halo mass of $M \sim 10^{13} h^{-1} M_{\odot}$ [solid line] can be compared with the empirical formula [dot dashed line] derived by Croom et al. (2005; see their equation 15) and with the model of Hopkings et al. (2007; see their equation 8) [dashed line]. The comparison shows that the three curves fit well the recent QSO bias evolution ($z < 2.5$). At higher redshifts ($z \geq 2.5$) our model evolves significantly more than the other two models, and it appears to be the only model that fits the recent, observationally derived, high- z QSO bias.

5. CONCLUSIONS

In this work we extend our original Basilakos & Plionis (2001) bias evolution model, based on linear perturbation theory and the Friedmann-Lemaître solutions of the cosmological field equations, to take into account the redshift evolution of an interaction term that could affect the mass-tracer number density. Parameterizing our analytical model with N-body simulations of the concordance Λ CDM cosmological model ($\Omega_m = 1 - \Omega_{\Lambda} = 0.3$), we investigate the halo-mass dependence of our linear bias evolution model, with or without the interaction term.

Assuming that the extragalactic mass tracers are hosted by a dark matter halo of given mass, we can predict analytically their present bias parameter and its z -evolution. Inversely, fitting our bias evolution model to the observed bias of different extragalactic mass-tracers, we can identify the typical mass of the DM halo within which they live.

Comparing our theoretical predictions with the observed bias of different mass-tracers (galaxies, AGNs, DRGs, EROs, etc) we find a very good agreement with our bias evolution functional form and therefore we also identify the typical mass of the DM halo which they inhabit. This has allowed us to infer that X-ray and optically selected AGNs inhabit DM halos of different mass (with X-ray AGNs being associated with higher DM halo masses).

REFERENCES

- Adelberger, K. L., Steidel, C. C., Giavalisco, M., Dickinson M., Pettini, M., & Kellogg, M., 1998, *ApJ*, 505, 18
 Arnouts, S., et al., 2002, *MNRAS*, 329, 355
 Bardeen, J.M., Bond, J.R., Kaiser, N. & Szalay, A.S., 1986, *ApJ*, 304, 15
 Bagla, J. S., 1998, *MNRAS*, 299, 417
 Basilakos, S. & Plionis, M., 2001, *ApJ*, 550, 522
 Basilakos, S. & Plionis, M., 2003, *ApJ*, 593, L61
 Basilakos, S., 2003, *ApJ*, 590, 636
 Basilakos, S., Georgakakis, A., Plionis, M., Georgantopoulos, I., 2004, *ApJ*, 607, L79
 Basilakos, S., Plionis, M., Georgakakis A., Georgantopoulos I., 2005, *MNRAS*, 356, 183
 Benson A. J., Cole S., Frenk S. C., Baugh M. C., Lacey G. C., 2000, *MNRAS*, 311, 793
 Catelan, P., Lucchin, F., Matarrese, S. & Porciani, C., 1998, *MNRAS*, 297, 692
 Cole, S., & Kaiser, N., 1989, *MNRAS*, 237, 1127
 Coles, P., Melott, A., Munshi, D., 1999, *ApJ*, 512, L5
 Croom, S. M., et al. 2005, *MNRAS*, 356, 415
 Davis, M., Efstathiou, G., Frenk, C. S., White, S D. M., 1985, *ApJ*, 292, 371
 Foucaud S., et al. 2007, *MNRAS*, 376, L20
 Fry J.N., 1996, *ApJ*, 461, 65
 Georgakakis A. Afonso J., Hopkins A. M., Sullivan M., Mobasher B., Cram L. E., *ApJ*, 2005, 620, 584
 Gilli, R., et al. 2005, *A&A*, 430, 811
 Grazian, A., et al. 2004, *AJ*, 127, 592
 Hopkins, P. F., Lidz, A., Hernquist, L., Coil, A. L., Myers, A. D., Cox, T. J., Spergel, D. N., 2007, *ApJ*, 662, 110
 Hui, L. & Parfrey, K.P., 2007, *Phys.Rev.D* *submitted*, [astro-ph/0712.1162](#)
 Jing, Y. P., 1998, *ApJ*, 503, L9
 Kaiser N., 1984, *ApJ*, 284, L9
 Kashikawa, N., et al., 2006, *ApJ*, 637, 631
 Kauffmann G., Golberg, J. M., Diaferio A., White S. D. M., 1999, *MNRAS*, 307, 529
 Lahav, O. et al., 2002, *MNRAS*, 333, 961
 Ma, Chung-Pei, & Fry, J. N., 2000, *ApJ*, 543, 503
 Magliocchetti M., et al., 2004, *MNRAS*, 350, 1485
 Marinoni, C., et al. 2005, *A&A*, 442, 801
 Matarrese, S., Coles, P., Lucchin, F., Moscardini, L., 1997, *MNRAS*, 286, 115
 Miyaji, T., et al., 2007, *ApJS*, 172, 396
 Mo, H.J, & White, S.D.M 1996, *MNRAS*, 282, 347
 Myers, A. D., Brunner, R. J., Nichol, R. C., Richards, G. T., Schneider D. P., Bahcall, N. A., 2007, *ApJ*, 658, 85
 Negrello, M., Magliocchetti, M., De Zotti, G., 2006, *MNRAS*, 368, 935
 Nusser, M., & Davis, M., 1994, *ApJ*, 421, L1
 Peacock, A. J., & Smith, E. R., 2000, *MNRAS*, 318, 1144
 Peebles P.J.E., 1993, *Principles of Physical Cosmology*, Princeton University Press, Princeton New Jersey
 Porciani, C., Magliocchetti, M., Norberg, P, 2004, *MNRAS*, 355, 1010
 Puccetti, S., et al., 2006, *A&A*, 457, 501
 Ragone-Figueroa, C., Plionis, M. 2007, *MNRAS*, 377, 1785

Roche D. N., Almaini O., Dunlop J., Ivinson J. R., Willot J. C., 2002, MNRAS, 337, 1282
 Seljak, U., 2000, MNRAS, 318, 203
 Seljak, U. & Warren, M.S., 2004, MNRAS, 355, 129
 Shen, Y., et al., 2007, AJ, 133, 2222
 Sheth R. K., & , Tormen, G., 1999, MNRAS, 308, 119
 Sheth, R. K., Diaferio, A., Hui, L., Scoccimarro, R., 2001 MNRAS, 326, 463
 Sheth R. K., Mo H. J., Tormen, G., 2001, MNRAS, 323, 1
 Silveira, V., & Waga, I., 1994, Phys. Rev. D, 64, 4890

Simon, P., 2005, A&A, 430, 827
 Somerville, R.S., Lemson, G., Sigad, Y., Dekel, A., Kauffmann, G., White, S.D.M., 2001, MNRAS, 320, 289
 Springel V., 2005, MNRAS, 364, 1105
 Steidel C.C., Adelberger L.K., Dickinson M., Giavalisco M., Pettini M., Kellogg M., 1998, ApJ, 492, 428
 Tegmark M., & Peebles P.J.E, 1998, ApJL, 500, L79
 Verde, L., et al. 2002, MNRAS, 335, 432
 Wang L., & Steinhardt P. J., 1998, ApJ, 508, 483

APPENDIX

REDSHIFT DEPENDENCE OF Ψ

With the aid of the Simon (2005) nomenclature we derive the expected redshift dependence of our interaction term $\Psi(z)$. In Simon (2005) the related ‘‘sink’’ term, $\phi(z)$, is modeled as the variation of the tracer number density, n_{tr} , given by their mass conservation equation:

$$\frac{dn_{tr}}{dt} + \frac{1}{a}\nabla(\mathbf{v}n_{tr}) = \phi \quad (\text{A1})$$

where a is the scale factor. Using the expression $n_{tr} = \bar{n}_{tr}(1 + \delta_{tr})$, in which \bar{n}_{tr} is the mean tracer density (depending on redshift), then the relation between ϕ and our Ψ function is given by:

$$|\Psi(t)| = \frac{1}{\bar{n}_{tr}(t)} \left[\phi(t) - (1 + \delta_{tr}) \frac{d\bar{n}_{tr}}{dt} \right] \quad (\text{A2})$$

Now, we can attempt to explore the functional form of our Ψ function, taking into account that the evolution of the galaxy luminosity function, $\Phi(L)$, can be parametrized ($k \sim 3$) as:

$$\Phi(L, z)dL = (1 + z)^k \Phi(L, 0)dL \quad (\text{A3})$$

Therefore, the corresponding mean density as a function of redshift becomes:

$$\bar{n}_{tr}(z) = (1 + z)^k \int_{L_{min}}^{\infty} \Phi(L)dL = \bar{n}_{tr}(0)(1 + z)^k \quad (\text{A4})$$

On the other hand, the time derivative of the mean density is written:

$$\frac{d\bar{n}_{tr}}{dt} = \frac{d\bar{n}_{tr}}{dz} \frac{dz}{dt} = -H_0 k \bar{n}_{tr}(0)(1 + z)^{k-1}(1 + z)E(z) = -kH_0 \bar{n}_{tr}(z)E(z) \quad (\text{A5})$$

Therefore we have that

$$|\Psi(z)| = \left[\frac{\phi(z)}{\bar{n}_{tr}(z)} + kH_0(1 + \delta_{tr}(z))E(z) \right] \quad (\text{A6})$$

In order to proceed, we make the following assumption (similar to that of Simon 2005), namely a Taylor expansion in $\bar{n}_{tr}(z)$ up to the second order:

$$\phi = A + B\bar{n}_{tr}(z) + C\bar{n}_{tr}^2(z) + \dots \quad (\text{A7})$$

with A, B and C constants. Doing so, eq.A6 becomes:

$$|\Psi(z)| \simeq \frac{A}{\bar{n}_{tr}(0)(1 + z)^k} + B + C\bar{n}_{tr}(0)(1 + z)^k + kH_0E(z) + kH_0E(z)\delta_{tr}(z) \quad (\text{A8})$$

or

$$|\Psi(z)| \simeq (1 + z)^k \left[\frac{A}{\bar{n}_{tr}(0)(1 + z)^{2k}} + \frac{B}{(1 + z)^k} + C\bar{n}_{tr}(0) + \frac{kH_0E(z)}{(1 + z)^k} + \frac{kH_0E(z)F(z)}{(1 + z)^{k+1}} \right] \quad (\text{A9})$$

where in the framework of the Λ cosmology, we have used that

$$\delta_{tr} \propto (1 + z)^{-1} F \left[\frac{1}{3}, 1, \frac{11}{6}, -\frac{\Omega_{\Lambda}}{\Omega_m(1 + z)^3} \right] \quad (\text{A10})$$

(see Silveira & Waga 1994) with $F(z)$ being the hypergeometric function which is an increasing function of redshift. Therefore, for $k \sim 3$ and at the high redshift limit, we have:

$$|\Psi(z)| \longrightarrow (1 + z)^3 \left[C\bar{n}_{tr}(0) + \frac{kH_0E(z)}{(1 + z)^3} \right] \quad (\text{A11})$$

while for the Einstein de Sitter universe:

$$|\Psi(z)| \longrightarrow (1 + z)^3 \left[C\bar{n}_{tr}(0) + \frac{kH_0}{(1 + z)^{3/2}} \right] \quad (\text{A12})$$

It is evident that the second term of the right hand-side of eqs. A11 and A12 is small at large redshifts, which implies that indeed, as we assumed in our model of Ψ (eq. 19 of main paper), $\Psi(z) \propto (1 + z)^{\nu}$. We also show analytically that we should expect $\nu \sim 3$, and indeed we find, fitting the simulation data, a similar value, ie., $\nu \sim 2.5$.

TABLE A1

FITTED *Case 2* BIAS EVOLUTION MODEL PARAMETERS AND THEIR 1σ UNCERTAINTIES, FOR DIFFERENT HALO-MASS RANGES. FOR THE S_4 AND S_5 SAMPLES, THE EFFECTS OF HALO INTERACTIONS IS NEGLIGIBLE AND THUS THE *Case 1* MODEL IS VALID.

Sample	$M/h^{-1}M_\odot$	\mathcal{C}_1	\mathcal{C}_2	χ^2/dof	b_0	A	ν
S_1	$7.7 \times 10^{11} - 1.0 \times 10^{13}$	2.12 ± 0.09	-0.24 ± 0.01	1.15	0.91 ± 0.01	$2 \pm 0.08 \times 10^{-3}$	2.56 ± 0.11
S_2	$1.0 \times 10^{13} - 3.0 \times 10^{13}$	3.98 ± 0.10	-0.43 ± 0.01	1.30	0.98 ± 0.02	$5 \pm 0.20 \times 10^{-3}$	2.62 ± 0.14
S_3	$3.0 \times 10^{13} - 6.0 \times 10^{13}$	5.48 ± 0.85	-0.57 ± 0.09	0.50	1.16 ± 0.04	$6 \pm 0.30 \times 10^{-3}$	2.54 ± 0.15
S_4	$6.0 \times 10^{13} - 1.0 \times 10^{14}$	6.78 ± 2.80	-0.68 ± 0.30	0.20	1.37 ± 0.10		
S_5	$1.0 \times 10^{14} - 4.0 \times 10^{14}$	9.09 ± 3.00	-0.89 ± 0.50	0.20	1.67 ± 0.10		